

Quantitative spatial mapping of distorted state phases during the metal-insulator phase transition for nanoscale VO₂ engineering

著者	ASHIDA Yuichi, ISHIBE Takafumi, YANG Jinfeng, NARUSE Nobuyasu, NAKAMURA Yoshiaki
journal or publication title	Science and Technology of Advanced Materials
volume	24
number	1
page range	1-9
year	2022-12-23
URL	http://hdl.handle.net/10422/00013537

doi: 10.1080/14686996.2022.2150525(<https://doi.org/10.1080/14686996.2022.2150525>)

Quantitative spatial mapping of distorted state phases during the metal-insulator phase transition for nanoscale VO₂ engineering

Yuichi Ashida^a, Takafumi Ishibe^b, Jinfeng Yang^b, Nobuyasu Naruse^c and Yoshiaki Nakamura^b

^aGraduate School of Engineering and Science, Osaka University, Toyonaka, Japan;

^bThe Institute of Scientific and Industrial Research, Osaka University, Ibaraki, Japan;

^cDepartment of Fundamental Bioscience, Shiga University of Medical Science, Otsu, Japan

ABSTRACT

Vanadium dioxide (VO₂) material, known for changing physical properties due to metal-insulator transition (MIT) near room temperature, has been reported to undergo a phase change depending on the strain. This fact can be a significant problem for nanoscale devices in VO₂, where the strain field covers a large area fraction, spatially non-uniform, and the amount of strain can vary during the MIT process. Direct measurement of the strain field distribution during MIT is expected to establish a methodology for material phase identification. We have demonstrated the effectiveness of geometric phase analysis (GPA), high-resolution transmission electron microscopy techniques, and transmission electron diffraction (TED). The GPA images show that the nanoregions of interest are under tensile strain conditions of less than 0.4% as well as a compressive strain of about 0.7% (Rutile phase VO₂[100] direction), indicating that the origin of the newly emerged TED spots in MIT contains a triclinic phase. This study provides a substantial understanding of the strain-temperature phase diagram and strain engineering strategies for effective phase management of nanoscale VO₂.

ARTICLE HISTORY

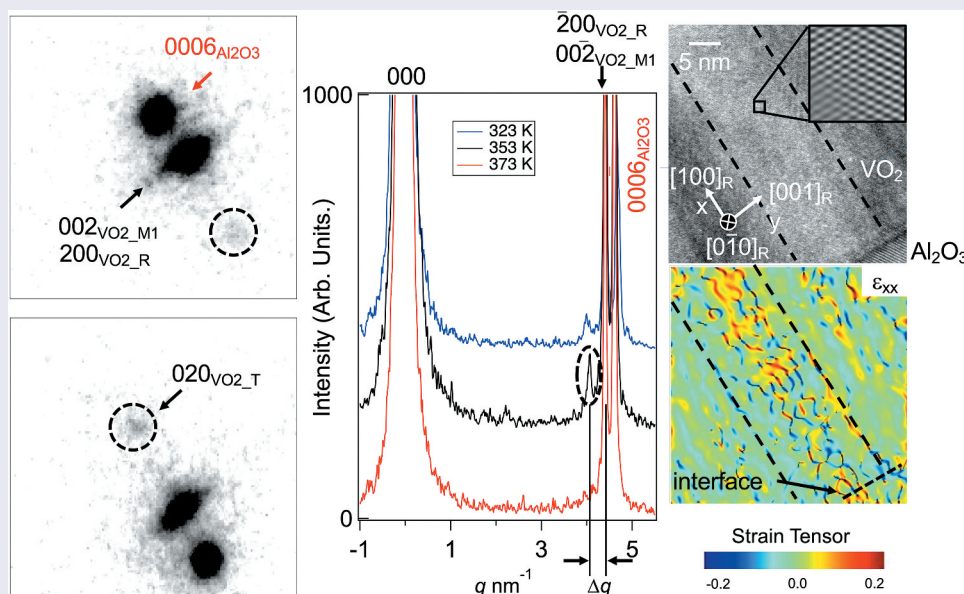
Received 1 September 2022

Revised 23 October 2022

Accepted 17 November 2022

KEYWORDS



VO₂ strained states; phase transition control; geometric phase analysis; VO₂ nanostructure




1. Introduction

Vanadium dioxide (VO₂) exhibits a metal-insulator transition (MIT) due to external fields such as heat [1,2], light [3,4], electric fields [5,6], and magnetic fields [7], which are accompanied by structural phase transition. In addition, strain [2,8,9], and doping [10–15] change the MIT conditions and properties. Since the electrical and optical properties of VO₂ change significantly with the phase transition, applications in

photonics and electronics are particularly promising [16–21]. Some optical switches have been developed combining VO₂ exhibiting the MIT with a silicon waveguide for miniaturizing optical switches [7]. The low-temperature VO₂ phases include not only the well-known M1 phase (monoclinic) but also two metastable structures, the insulating M2 phase (monoclinic) and T phase (triclinic), due to stoichiometric defects and strain effects, which can pose challenges

CONTACT Nobuyasu Naruse  naruse@belle.shiga-med.ac.jp  Department of Fundamental Bioscience, Shiga University of Medical Science, Otsu, Japan

 Supplemental data for this article can be accessed online at <https://doi.org/10.1080/14686996.2022.2150525>

© 2022 The Author(s). Published by National Institute for Materials Science in partnership with Taylor & Francis Group.

This is an Open Access article distributed under the terms of the Creative Commons Attribution License (<http://creativecommons.org/licenses/by/4.0/>), which permits unrestricted use, distribution, and reproduction in any medium, provided the original work is properly cited.

for nanoscale devices [22,23]. Due to their metastable structures and spatial phase inhomogeneities in the film/bulk samples, these structural phases can exhibit different phase transition behaviors and properties. In recent years, a wide range of device applications involving miniaturization using nanostructures and nanofilms of oxides have been expanding [24–26]. Precise control of domain structures and phase transitions at the single domain level is also expected for VO₂ materials, and the development of a method to precisely characterize the phase structure of VO₂ at the nanoscale is a major challenge [27].

According to Wang *et al.* [28] and Kim *et al.* [29], the M2 and T phases are stabilized by doping, external strain, and oxygen nonstoichiometry. Effective strain control strategies are necessary to create VO₂ crystals with stabilized multiphase because doping and stoichiometry can cause large structural distortions in the VO₂ lattice, changing its intrinsic properties and applications. Strained VO₂ fields are not a problem in conventional macroscopic devices but are critical in nanoscale devices; the area covered by the strained field is large and spatially non-uniform, and the amount of strain can change during the phase transition process. However, the challenge is that there is no way to quantitatively measure the strain state of those VO₂ in actual nanomaterials.

In this study, using geometric phase analysis (GPA), an analysis of high-resolution electron microscopy (HRTEM), we have exhibited crystallographic evidence from transmission electron diffraction (TED) that there is indeed an intermediate phase of the MIT while quantitatively evaluating the strain in thin films of VO₂ grown on sapphire. In order to precisely control VO₂ and even the properties of the phase transition process in the future, we need a recipe to quantitatively measure the strain of the desired nanostructure. We will demonstrate that GPA and TED can be used to quantitatively evaluate the strain of phase transitions in the single domain, which was not readily apparent due to the sub-resolution displacement of HRTEM.

2. Experimental details

A c-cut sapphire substrate (10 × 10 mm²) was ultrasonically cleaned with acetone, ethanol, and an ultrapure water bath for 5 min each. After removing the surface moisture with a nitrogen gun, the washed sample was introduced into a load lock chamber. Then, the sample was transferred to a deposition chamber equipped with a pulse laser deposition system (Lambda Physics) [25]. A V₂O₅ target was used for the growth of VO₂ film. The deposition chamber was evacuated to a 2×10^{-5} Pa prior to deposition. The thickness of the VO₂ thin film of 100 nm was formed on the substrate by pulsed ArF laser deposition (wavelength 248 nm,

energy 50 mJ, frequency 10 Hz, substrate temperature 723 K, O₂ pressure 1.0 Pa). The temperature dependence of the electrical conductivity of the VO₂ film was measured between 300 and 400 K by the van der Pauw method (self-made) to confirm the phase transition temperature (Supporting information Figure S1 (a)). The crystallinity of the fabricated VO₂ film was evaluated by X-ray diffraction (XRD) measurements (Rigaku, Ultima IV) with 2θ-ω scan (Supporting information Figure S1(b)).

Focused ion beam processing (Thermo Fisher Scientific, Scios 2) was performed to thin the VO₂ film so that it could be observed from [010]_{M1} (Rutile phase VO₂[010]_R) orientation. The TED pattern and cross-sectional HRTEM were taken at 200 keV (HITACHI, HF-2000). The temperature was repeatedly lowered and raised 323–373 K (323 K, 353 K, 373 K) in the TEM with a temperature variable holder (Gatan, 628). The temperature was held for about 15 minutes until each temperature became constant, and then HRTEM and TED observations were performed. There was no significant change in the diffraction pattern at the same temperature when the temperature was raised and lowered. Geometric Phase Analysis (GPA) was used to visualize the strain changes in the VO₂ film using Grillo's algorithm STEM_cell [30]. The diffracted spots of VO₂ (002)_{M1} and (202)_{M1} were used as reference points for the GPA. The output GPA images are 16 bits.

3. Results and discussion

The TED pattern shown in Figure 1(a) is taken from VO₂[010]_{M1} (VO₂[010]_R and Al₂O₃[1120]) direction, which allows us for detailed measurements of the atomic arrangement changes in M1, M2, T, and R phases. The R phase is known as metallic. The pattern was obtained at 353 K from a 5 μm VO₂ thin film region together with the sapphire substrate as a reference for d-spacing. As shown in the cross-sectional TEM image (Figure 1(b)) of a VO₂ film formed on the substrate, VO₂ domains grow perpendicular to the interface. Although it is difficult to see in the wide-area TEM image in Figure 1(b), the VO₂ domain is 10–20 nm size in parallel to the interface and is long in the surface direction. Figure 1(c–f) are enlarged images of the area enclosed by the square at 353 K and 373 K. These spots are indexed as 200_{VO2_R} and $\bar{2}00_{VO2_R}$. When the sample temperature is further lowered to 353 K from 373 K, the intensity of the newly emerging spots, which could hardly be visualized at 373 K, becomes more intense. The spots appeared along the line parallel to the [100]_R direction; it was observed as a strong intensity at 353 K and as a small intensity at 323 K. Streaky diffraction spots

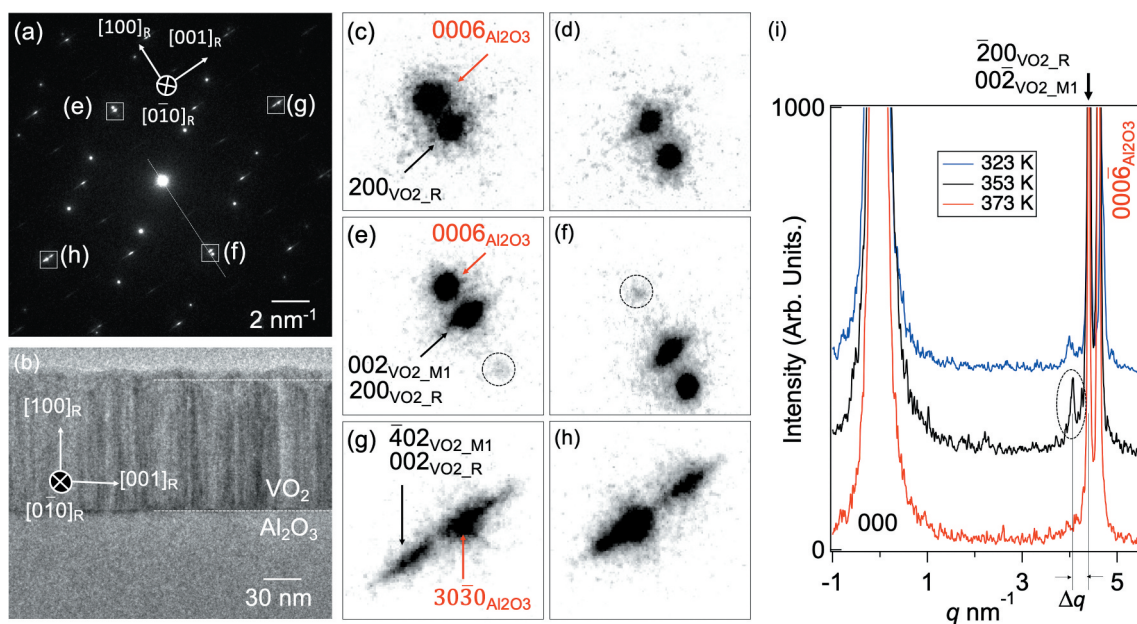


Figure 1. (a) TED pattern viewed from $\text{VO}_2[0\bar{1}0]_R$ and $\text{Al}_2\text{O}_3[11\bar{2}0]$ direction at 353 K. (b) A cross-sectional TEM image for VO_2 film on Al_2O_3 substrate. The magnified image of the SAED around (c) the spot of $200_{\text{VO}_2\text{-R}}$ and (d) $\bar{2}00_{\text{VO}_2\text{-R}}$ at 373 K. (e) and (f) Diffraction spots at 353 K for the same spots as (c) and (d). The diffraction spots surrounded by a circular dotted line appeared only at 353 K. (g) and (h) Magnified image around $402_{\text{VO}_2\text{-M1}}$ ($002_{\text{VO}_2\text{-R}}$) and $30\bar{3}0_{\text{Al}_2\text{O}_3}$ spots at 353 K. (i) Line profile of the white dotted line in (a) at the temperature of 353 K. The distance Δq between the $\bar{2}00_{\text{VO}_2\text{-R}}$ spot and the newly appeared one on the reciprocal space is 0.34 nm^{-1} .

were observed parallel to the $\text{VO}_2[001]_R$ direction (Figure 1(g,h)). The streak spots correspond to the presence of a VO_2 single domain with a width of 10–20 nm. The domain size was also confirmed by atomic force microscopy images of the surface (Supporting information Figure S2).

There are two possible explanations for the newly emerging spots. One explanation is that the VO_2 domain has a T phase with the M1 and R phases due to a strain. The relationship between temperature and strain proposed by Raman spectroscopy has suggested that VO_2 becomes T phase at 0.5–1% relative strain [31]. Another explanation is the generation of a new long-period strained structure, as discussed later. First, we consider the former in detail. Assuming that the newly emerged spots are the lattice spacing (d-spacing) of the new crystal phase, it corresponds to $d = 0.24 \pm 0.05 \text{ nm}$. According to the previous reports of XRD, the emerging spots correspond to $020_{\text{VO}_2\text{-T}}$ on reciprocal space [11,12]. There is no evidence as to how strained the VO_2 domains are at 353 K, although it has been reported that the area near the interface with sapphire is under a strain state [32]. However, the difference in the arrangement of V atoms between M1, M2, and T phases is reported to be smaller than 0.02 nm, which is difficult to distinguish even with the help of HRTEM image simulations. In addition, the XRD of the T phase was measured by creating a strained state by doping with Al [23], which can be different from the phase caused by external pressure or force fields.

Moreover, the biggest question is why the spots that appeared at 353 K were not observed at 323 K.

Next, to check the strain state at 353 K, GPA was performed for the acquired HRTEM images. The lattice mismatch between the VO_2 (M1 and R phases) and $\text{Al}_2\text{O}_3(0001)$ substrates is 4.50% and 4.92% parallel to the interface, respectively. Figure 2(a–c) are HRTEM images of the vicinity of the substrate at each temperature. Figure 2(d–i) are GPA images at each temperature and orientation. The inset shows the FFT image of the region surrounded by the white dashed line in Figure 2(a–c). The black dashed line is the boundary of a single crystal domain of VO_2 . The $\text{VO}_2[100]_R$ direction along the domain boundary is the x-axis of the strain component, and the $\text{VO}_2[001]_R$ direction is the y-axis. Strain components ϵ_{xx} and ϵ_{yy} visualize the strain state in the VO_2 domain. Especially in 353 K the distortion is concentrated in the central domain of the ϵ_{xx} image, which is only under the compressive strain of below 0.7% but also under the tensile strain of 0.2% (Figure 3). Although the strain is almost zero on average in 353 K, the width of the peak is broader, i.e. the area containing the tensile strain is -0.7 to $+0.4\%$. The ϵ_{yy} images showed that the strains are concentrated near the interface. The compressive strain applied in the x-direction change significantly at each of the temperatures of 323 K and 373 K. This VO_2 thin film is formed so that nanorods are growing in the x-direction. As shown in Figure 4(a,b), The change from the M1

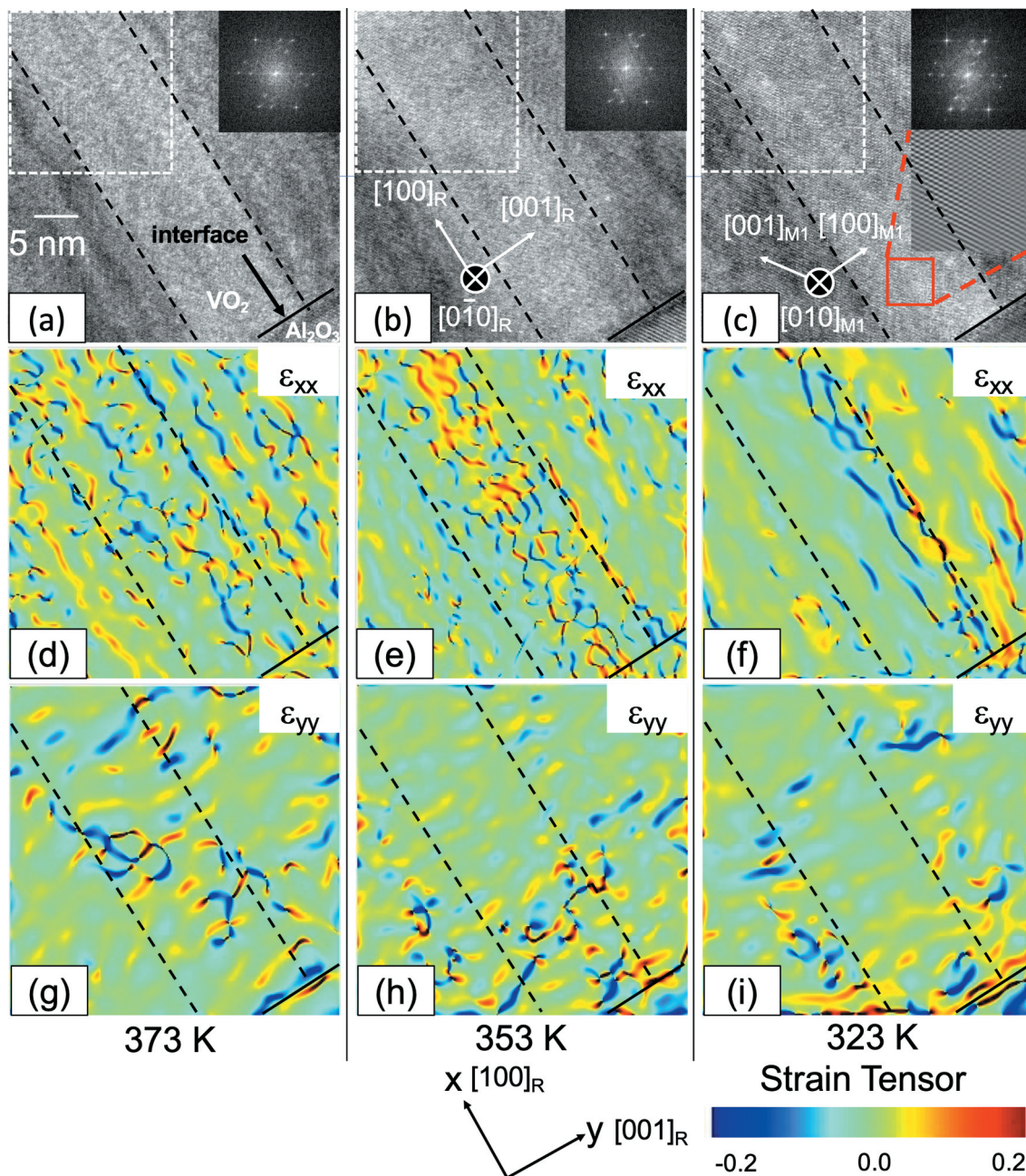


Figure 2. HRTEM images VO₂ film area together with the interface with Al₂O₃ substrate at (a) 373 K, (b) 353 K, and (c) 323 K, respectively. The insets of FFT images were from the area surrounded by the white dashed line. The inset of HRTEM image in (c) shows a magnified image of the red square region, indicating that those HRTEM images are of sufficient quality to perform a geometric phase analysis (GPA) (Supporting information Figure 3S(a–c)). Strain mapping of different strain terms along the (d)–(f) ϵ_{xx} direction (VO₂[100]_R) and (g)–(i) ϵ_{yy} direction (VO₂[001]_R) between (002)_{M1} and (402)_{M1} were obtained by GPA of the HRTEM images at the respective temperature. Black dashed lines in (a)–(i) indicate the VO₂ domain wall. Solid black lines exhibit the interface between VO₂ film and Al₂O₃ substrate.

phase to the R phase (or vice versa) is accompanied by a volume change that changes the angle and the lattice constant. In the x-direction, there is a space in which the crystal volume change is possible. However, for the y-direction, a phase transition with a large volume change is difficult because another VO₂ domain exists right next to those. This can result in increased compressive strain with anisotropy at 373 K, as shown in Figure 5(b). As shown in Figure 3, both compressive and tensile strains are present at 323K in the nanoscale range, but they are offset in total. This situation may be

the reason for the wide range in strains, although it is plotted where there are no strains in total at 323 K, as shown in Figure 5(b).

To interpret the results of all the above analyses, the atomic arrangement of the T phase was considered together with that of the M1 and R phases. A schematic diagram of V atoms shifts in the M1-R phase transition is illustrated in Figure 4(a). As is well known, the V atoms aligned in the c-axis direction of the rutile-type structure form a zigzag chain at low temperatures, with the V atoms alternately shifting by

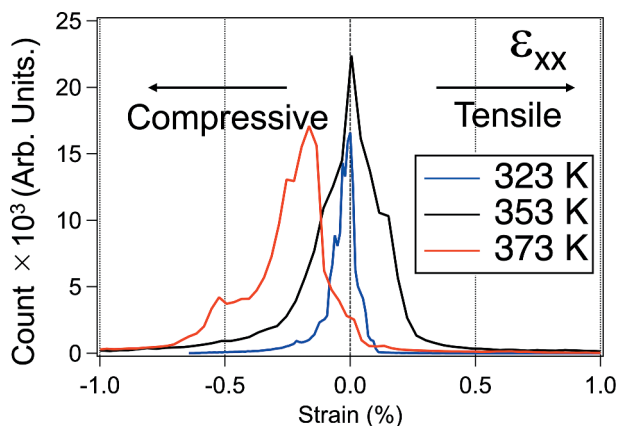


Figure 3. Histograms of strain in the ϵ_{xx} direction in the area sandwiched by the domain boundary in Figure 2(d–f).

0.02 nm. This structural change reduces the symmetry and changes the structure from Tetragonal to Monoclinic. The lattice spacing of $d(002)_{M1}$ and $d(200)_R$ is almost equal, 0.227 nm. In contrast, the structural models of the M1 phase (blue) and T phase (orange) focusing on the shift of V atoms are illustrated in Figure 4(b), although the slight difference in angle is not shown. Compared to the M1 phase, the T phase has a zigzag sequence of V atoms every other row. The lattice spacing of $d(020)_T$ is 0.243 nm, corresponding to 4.1 nm^{-1} in reciprocal space. The peaks of XRD between $2\theta = 36$ and 44 degrees in previous works of $\text{VO}_2(\text{M2})$ [22], $\text{VO}_2(\text{T})$ [12], and $\text{VO}_2(\text{R})$ [33] are shown in Figure 5(a) (Full range XRD data are shown in Supporting Information,

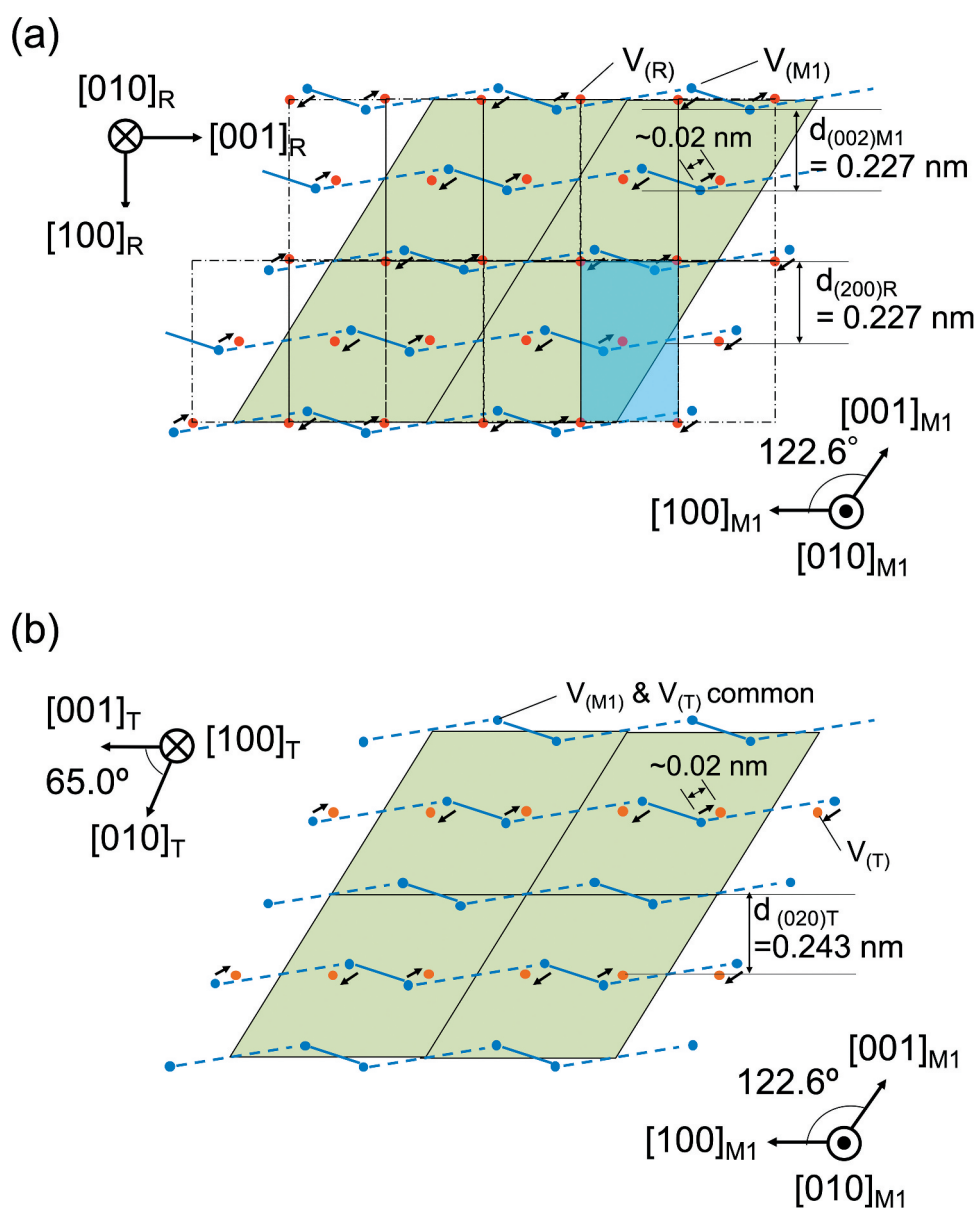


Figure 4. (a) Schematic diagram of V atoms shifts in M1-R phase transition (the spheres indicate positions of the vanadium atoms in the R (red) and M1 (blue) phases). Blue solid lines and dashed blue lines represent the short and long bond lengths. The unit cell for phase R is shown as a blue rectangle, and the unit cell for phase M1 is a green parallelogram. The V-atomic shift is 0.02 nm. The lattice spacing of $d(002)_{M1}$ and $d(200)_R$ is almost the same, 0.227 nm. (b) Structural model of M1 (blue) and T (orange) phases focusing on V atoms shift. Slit angle differences in the structural model are not shown. Compared to the M1 phase, the T phase has a zigzag chain of V atoms every other row. The lattice spacing of $d(020)_T$ is 0.243 nm, corresponding to 4.1 nm^{-1} .

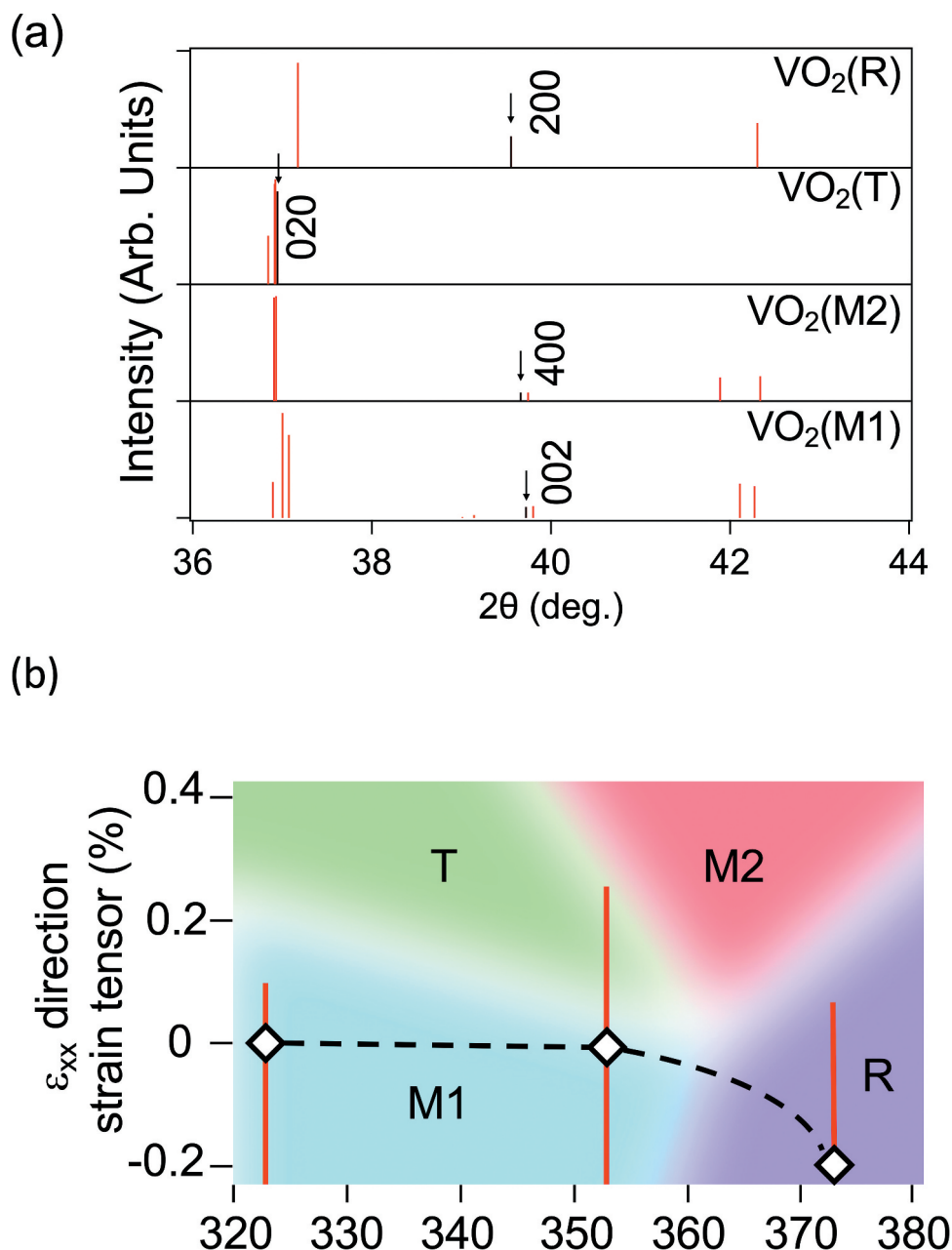


Figure 5. (a) XRD peaks between $2\theta = 36$ and 44 degrees in JCPDS plots of VO₂ (M1) and reported previous works of VO₂(M2) [22], VO₂(T) [12], and VO₂(R) [33]. The black lines in stand for Bragg peaks that can be appeared in the spots of Figure 1(c–f). (b) Strain-temperature phase diagram of VO₂ suggested by D. H. Cobden *et al.* (modified) [34]. The diamond marks indicate the averaged strain deduced by GPA. The length of the bars indicates more than 2000 counts shown in Figure 3. The dotted line means an estimated change in average strain during the phase transition process.

Figure S5). The black lines in Figure 5(a) stand for Bragg peaks that can be appeared in the TED spots of Figure 1(c–f).

The zigzag chains of the T phase are aligned perpendicular to the [100]_R direction every cycle, which can be considered as stacking defects generated during the phase transition from R to M1. The T phase can be mixed with the M1 as a metastable structure. While the angle β of the unit cell in the M1 phase is 122.6 degrees, the corresponding angle in the T phase is angle α , which is 65.0 degrees (supporting information Table S1). Since the obtuse angle of the parallelogram of the unit cell of the M1 phase is wider in the T, this

structural change in the T compared to the M1 means that the volume change in the x-axis direction, that is, the direction parallel to the [100]_R direction, is more prominent. This difference in the angle of the structural phase is consistent with the fact that the VO₂ domains at 353 and 373 K are more strained in both parallel and perpendicular directions in the [100]_R direction than those in the M1 phase, especially compressive strain at higher temperatures.

The major difference between the characteristics of phase transitions on the nanoscale and those on the microscale is that the amount and type of strain can change during the phase transition process. The

modified strain-temperature phase diagram for VO₂ proposed by D. H. Cobden *et al.* is shown in Figure 5(b) [34]. Since their results were obtained by Raman spectroscopy at the microscale under external stress, the metastable T phase can be observed at the nanoscale even under low strain states. The diamond marks stand for the strain peaks in Figure 3. The bar is in the range of 2000 counts or more in the histogram obtained from our GPA (Figure 3). The dotted line means an estimated change in average strain during the phase transition process. If a region of M2 phase existed in our samples, a diffraction spot of VO₂(400)_{M2} should appear at 373 K as shown in Figure 5(a). However, the spot did not appear in the actual TED pattern. This suggests a single rutile phase at 373 K. Our measurements suggest that the degree of strain depends on the external field in the structural phase transition process of VO₂, implying that the control of the single domain or nanostructure is crucial.

Finally, we discuss the possibility of generating a new strain long-period structure as described in the previous paragraph. The strained component appears to have a superstructure with a period of 0.24 nm, corresponding to 4 nm⁻¹ in reciprocal space (shown in supporting information, Figure S4). This period is close to the value of Δq shown in Figure 1(i). However, if a long-period structure occurred, a peak should also appear near the 000-transparent spot, but no clear peak was observed. Assuming that a long-period strain exists in the x-direction (VO₂[100]_R), its half-period is 4 ± 0.5 nm, as shown in Figure S4. In reciprocal space, this value corresponds to 0.222–0.285 nm⁻¹. Even if spots due to long-period strain appear, they should be broad, not the sharply peaked spots observed here. Indeed, the corresponding peaks were not identified in the line profiles obtained from the fast Fourier transform (FFT) for the HRTEM image (Figure S3 (e)). Therefore, the possibility of a long-period structure of strain was ruled out.

The GPA in this study directly shows that an obstacle in the direction of the volume change associated with the phase transition causes strains in the VO₂ nanocrystal, which in turn affects the phase transition phase. Due to the strain caused by the lattice mismatch between the sapphire substrate interface and VO₂, it has been reported that strains are internalized at the interface. The strains act to lower the phase transition temperature of MIT [2]. These reports refer to the structural phase change within only 10 nm from the interface; however, there is no direct indication that strains can occur in the structural phase transition process of the entire domain shown in this study. There was a large difference in the change rate of electrical conductivity near the high-temperature phase and near the low-temperature phase of VO₂ (Supporting information Figure S1(a)). The mixture of the two phases in the low-temperature phase may

cause this difference. Stable and precise control of the phase structure of VO₂ is essential to fabricate the desired nanostructure. We believe that this study is of great significance as it demonstrates the possibility of controlling the intermediate phase of VO₂ in the future. Recently, VO₂ materials have been considered promising candidates for optical switches, which undergo ultrafast light-induced structural phase transitions on the order of 100 femtoseconds [3,4,35–38]. However, little analysis has been done taking strain into account. Our study also suggests that it is meaningful to evaluate the implied strain when tracing the structural changes in VO₂ induced by ultrafast pulsed light irradiation.

4. Conclusion

In conclusion, we have provided crystallographic evidence by electron diffraction that the MIT intermediate phase exists while quantitatively characterizing the strain in VO₂ thin film grown on sapphire using GPA. The new diffraction spots at 353 K suggested the presence of a phase with the d-spacing of 0.243 nm (4.1 nm⁻¹) in the [100]_R orientation. The GPA shows the tensile strain of -0.7 to +0.4% (Rutile phase VO₂[100] direction) in the single domain at 353 K and 373 K compared to that at 323 K, which may cause the T phase to hybridize with the M1 phase. Those methods used in this study could be helpful for precise control of the nanostructure of VO₂, monitoring the variable strain field during the phase transition process in a nanoscale domain.

Disclosure statement

No potential conflict of interest was reported by the authors.

Funding

This work was partially supported by Grant-in-Aid for Scientific Research (A) Grant number [21H04654], Nanotechnology Platform of MEXT, Grant Number [JPMXP09S21OS0011]. A part of this work was supported by Advanced Characterization Nanotechnology Platform, Nanotechnology Platform Program of the Ministry of Education, Culture, Sports, Science and Technology (MEXT), Japan, Grant Number [JPMXP09A21OS0013] at the Research Center for Ultra-High Voltage Electron Microscopy (Nanotechnology Open Facilities) in Osaka University.

ORCID

Takafumi Ishibe  <http://orcid.org/0000-0002-8662-875X>

Jinfeng Yang  <http://orcid.org/0000-0001-5034-3982>

Nobuyasu Naruse  <http://orcid.org/0000-0003-3934-2641>

Yoshiaki Nakamura  <http://orcid.org/0000-0002-5387-1630>

References

- [1] Morin FJ. Oxides which show a metal-to-insulator transition at the Neel temperature. *Phys Rev Lett.* 1959;3(1):34.
- [2] Théry V, Boulle A, Crunteanu A, et al. Role of thermal strain in the metal-insulator and structural phase transition of epitaxial VO₂ films. *Phys Rev B.* 2016;93(18):184106.
- [3] Morrison VR, Chatelain RP, Tiwari KL, et al. A photoinduced metal-like phase of monoclinic VO₂ revealed by ultrafast electron diffraction. *Science.* 2014;346(6208):445.
- [4] Wall S, Yang S, Vidas L, et al. Ultrafast disordering of vanadium dimers in photoexcited VO₂. *Science.* 2018;362(6414):572.
- [5] Nakano M, Shibuya K, Okuyama D, et al. Collective bulk carrier delocalization driven by electrostatic surface charge accumulation. *Nature.* 2012;487(7408):459.
- [6] Chen Y, Wang Z, Chen S, et al. Electric-field control of Li-doping induced phase transition in VO₂ film with crystal facet-dependence. *Nano Energy.* 2018;51:300.
- [7] Matsuda YH, Nakamura D, Ikeda A, et al. Magnetic-field-induced insulator-metal transition in W-doped VO₂ at 500 T. *Nat Commun.* 2020;11(1):1.
- [8] Fan LL, Chen S, Luo ZL, et al. Strain dynamics of ultrathin VO₂ film grown on TiO₂ (001) and the associated phase transition modulation. *Nano Lett.* 2014;14(7):4036.
- [9] Yang M, Yang Y, Hong B, et al. Surface-growth-mode-induced strain effects on the metal-insulator transition in epitaxial vanadium dioxide thin films. *RSC Adv.* 2015;5(98):80122.
- [10] Ling C, Zhao Z, Hu X, et al. W doping and voltage driven metal-insulator transition in VO₂ nano-films for smart switching devices. *ACS Appl Nano Mater.* 2019;2(10):6738.
- [11] Shibuya K, Okuyama D, Kumai R, et al. X-ray induced insulator-metal transition in a thin film of electron-doped VO₂. *Phys Rev B.* 2011;84(16):165108.
- [12] Andreev VN, Klimov VA, Kompan ME, et al. Specific features of hydrogenation of chromium-doped polycrystalline thin vanadium dioxide films. *Phys Solid State.* 2014;56(9):1857.
- [13] Strelcov E, Tselev A, Ivanov I, et al. Doping-based stabilization of the M2 phase in free-standing VO₂ nanostructures at room temperature. *Nano Lett.* 2012;12(12):6198.
- [14] Hanlon TJ, Coath JA, Richardson MA. Molybdenum-doped vanadium dioxide coatings on glass produced by the aqueous sol-gel method. *Thin Solid Films.* 2003;436(2):269.
- [15] Lu L, Wu Z, Ji C, et al. Effect of Fe doping on thermochromic properties of VO₂ films. *J Mater Sci.* 2018;29(7):5501.
- [16] Markov P, Marvel RE, Conley HJ, et al. Optically monitored electrical switching in VO₂. *ACS Photonics.* 2015;2(8):1175.
- [17] Joushaghani A, Jeong J, Paradis S, et al. Wavelength-size hybrid Si-VO₂ waveguide electroabsorption optical switches and photodetectors. *Opt Express.* 2015;23(3):3657.
- [18] Sadeghi M, Janjan B, Heidari M, et al. Mid-infrared hybrid Si/VO₂ modulator electrically driven by graphene electrodes. *Opt Express.* 2020;28(7):9198.
- [19] Sanchez L, Rosa A, Griol A, et al. Thermo-optical switching in hybrid VO₂/Si waveguides by lateral displaced microheaters. 14th International Conference on Group IV Photonics, GFP; Grand Hyatt Berlin, Germany; 2017. p. 41.
- [20] Sánchez, LD, Rosa A, Angelova T, et al. Electrical switching in hybrid VO₂/Si photonic structures. International Conference on Transparent Optical Networks; Trento, Italy; 2016. p. 1.
- [21] Shiga D, Yang BE, Hasegawa N, et al. Thickness dependence of electronic structures in VO₂ ultrathin films: suppression of the cooperative Mott-Peierls transition. *Phys Rev B.* 2020;102(11):115114.
- [22] Chamberland BL. New defect vanadium dioxide phases. *J Solid State Chem.* 1973;7:377.
- [23] Ghedira M, Vincent H, Marezio M, et al. Structural aspects of the metal-insulator transitions in V_{0.985}Al_{0.015}O₂. *J Solid State Chem.* 1977;22(4):423.
- [24] Ishibe T, Taniguchi T, Terada T, et al. Areal density control of ZnO nanowires in physical vapor transport using Ge nanocrystals. *Jpn J Appl Phys.* 2018;57(8S1):08NB07.
- [25] Tomeda A, Ishibe T, Taniguchi T, et al. Enhanced thermoelectric performance of Ga-doped ZnO film by controlling crystal quality for transparent thermoelectric films. *Thin Solid Films.* 2018;666:185.
- [26] Ishibe T, Tomeda A, Watanabe K, et al. Embedded-ZnO nanowire structure for high-performance transparent thermoelectric materials. *J Electron Mater.* 2017;46(5):3020.
- [27] Takami H, Kawatani K, Ueda H, et al. Tuning metal-insulator transition by one dimensional alignment of giant electronic domains in artificially size-controlled epitaxial VO₂ wires. *Appl Phys Lett.* 2012;101(26):263111.
- [28] Wang Y, Sun X, Chen Z, et al. Defect-engineered epitaxial VO₂±δ in strain engineering of heterogeneous soft crystals. *Sci Adv.* 2018;4(5):1.
- [29] Kim MW, Ha SS, Seo O, et al. Real-time structural and electrical characterization of metal-insulator transition in strain-modulated single-phase VO₂ wires with controlled diameters. *Nano Lett.* 2016;16(7):4074.
- [30] Grillo V, Rossi F. STEM_CELL: a software tool for electron microscopy. Part 2 analysis of crystalline materials. *Ultramicroscopy.* 2013;125:112.
- [31] Atkin JM, Berweger S, Chavez EK, et al. Strain and temperature dependence of the insulating phases of VO₂ near the metal-insulator transition. *Phys Rev B.* 2012;85(2):020101.
- [32] He X, Xu T, Xu X, et al. In situ atom scale visualization of domain wall dynamics in VO₂ insulator-metal phase transition. *Sci Rep.* 2014;4(1):6544.
- [33] Akroune A, Claverie J, Tazairt A, et al. Propriétés structurales, magnétiques et électriques des oxyfluorures V_{1-x}M_xO_{2-2x}F_{2x} (M = Mg, Ni). *Phys Status Solidi (a).* 1985;89:271.
- [34] Park JH, Coy JM, Serkan Kasirga T, et al. Measurement of a solid-state triple point at the metal-insulator transition in VO₂. *Nature.* 2013;500(7463):431.

- [35] Yang J, Gen K, Naruse N, et al. A compact ultrafast electron diffractometer with relativistic femtosecond electron pulses. *Quantum Beam Sci.* **2020**;4(1):4.
- [36] Muro’Oka Y, Naruse N, Sakakihara S, et al. Transmission-electron diffraction by MeV electron pulses. *Appl Phys Lett.* **2011**;98(25):251903.
- [37] Daraszewicz SL, Giret Y, Naruse N, et al. Structural dynamics of laser-irradiated gold nanofilms. *Phys Rev B.* **2013**;88(18):184101.
- [38] Giret Y, Naruse N, Daraszewicz SL, et al. Determination of transient atomic structure of laser-excited materials from time-resolved diffraction data. *Appl Phys Lett.* **2013**;103(25):253107.